Earth and Planetary Science Letters ••• (••••) ••••••

Contents lists available at ScienceDirect

Earth and Planetary Science Letters

www.elsevier.com/locate/epsl

Plate-driven micro-hotspots and the evolution of the Dragon Flag melting anomaly, Southwest Indian Ridge

Xing Yu [a,b,*], Henry J.B. Dick [b]

[a] Key Laboratory of Submarine Geosciences, State Oceanic Administration, Second Institute of Oceanography, Ministry of Natural Resources, Hangzhou 310012, China

[b] Department of Geology and Geophysics, Woods Hole Oceanographic Institution, Woods Hole, MA 02543, USA

ARTICLE INFO

Article history:
Received 21 March 2019
Received in revised form 28 November 2019
Accepted 2 December 2019
Available online xxxx
Editor: F. Moynier

Keywords:
Southwest Indian Ridge
melting anomaly
magma evolution
heterogeneity
micro-hotspot
ridge-hotspot interaction

ABSTRACT

Micro hotspots represent excess volcanism at the ultraslow spreading Southwest Indian Ridge (SWIR) unrelated to mantle hotspots, but to focused melt flow in the mantle, wide volcano spacing, and/or increased mantle fertility. Individual micro hotspot can reflect variations in regional mantle fertility, simultaneously affecting 100's of km of ridge, or extreme melt focusing to isolated segments in regions with unusually thick lithosphere. The Dragon Flag melting anomaly, erupting isotopically moderately depleted low-K tholeiite, is the best example of the former: an enormous ridge-centered volcano at 50.5°E. It is far from Crozet, and lies at the apex of a V-shaped trace consisting of ~1 km anomalously elevated seafloor that extends ~400 km to the northwest and southeast, indicating a sudden onset of excess volcanism at ~11-8 Ma. This trend is opposite to that predicted by the hotspot framework, with inconsistent geochemistry. Narrowgate at 14.7°E is one of many micro hotspots that represent isolated large volcanic centers bounded by long amagmatic ridge sections. It also lies at the apex of an eastward V-shaped bathymetric trend, but erupts large volumes of alkali basalt.

Both micro hotspot varieties are an order of magnitude smaller than Wilson's classic hotspots, and are not fixed in the hotspot referenced frame. They can grow and remain stationary for extended periods, or migrate freely with respect to each other; driven by the evolving plate tectonic stress field. Dragon Flag, represents a plate reorganization during a prolong period of enhanced melt supply. Narrowgate, on the other hand represents excess volcanism due to extreme deep melt focusing of low degree melt from an unusually wide region in the mantle to an isolated volcanic segment where thick lithosphere caps melting at great depth. To constrain the origins of the micro hotspots six examples are evaluated in terms of their major and isotopic composition, prior plate history, depth and extent of melting and tectonic context. This includes new major, trace element, and heavy isotope data for the Dragon Flag Supersegment, and unpublished data for the Joseph Mayes and Narrowgate segments.

© 2019 Elsevier B.V. All rights reserved.

1. Introduction

While the isotopic mantle heterogeneity occurs globally at all scales, from grain size to hemisphere (Anderson, 2006), that observed in the SWIR is exceptional, both laterally and locally (le Roex et al., 1989; Mahoney et al., 1992; Janney et al., 2005; Standish, 2006; Gautheron et al., 2015; Gao et al., 2016). The crust along the Southwest Indian Ridge (SWIR) is generally thin and discontinuous, with the mantle spreading directly to the seafloor in many regions (Zhou and Dick, 2013), there are also areas, micro hotspots, where it is up to 10 km thick. These differ widely in their geometry and geochemistry. The cause of the melting anomaly could be due to many possibilities: (1) the influence of mantle plumes, including Marion and Crozet (e.g. Georgen et al., 2001); (2) mantle source modification by subduction with sediments and oceanic crust (e.g. Rehkämper and Hofmann, 1997; Kempton et al., 2002); (3) stranded lower continental crust/continental lithospheric mantle mixed with the upper mantle (e.g. Meyzen et al., 2005; Mahoney et al., 1992; Janney et al., 2005).

Meyzen et al. (2005), based on MORB $^{87}Sr/^{86}Sr$, $^{143}Nd/^{144}Nd$ and $^{206}Pb/^{204}Pb$ isotopes, suggest that there was no influence of the Marion and Crozet mantle plumes on the supersegment. Moreover, Dalton et al. (2014) also suggest no significant plume influence on the supersegment due to the relatively low mantle potential temperature estimated from seismic tomography and

* Corresponding author.
E-mail address: yuxing@sio.org.cn (X. Yu).

https://doi.org/10.1016/j.epsl.2019.116002
0012-821X/© 2019 Elsevier B.V. All rights reserved.

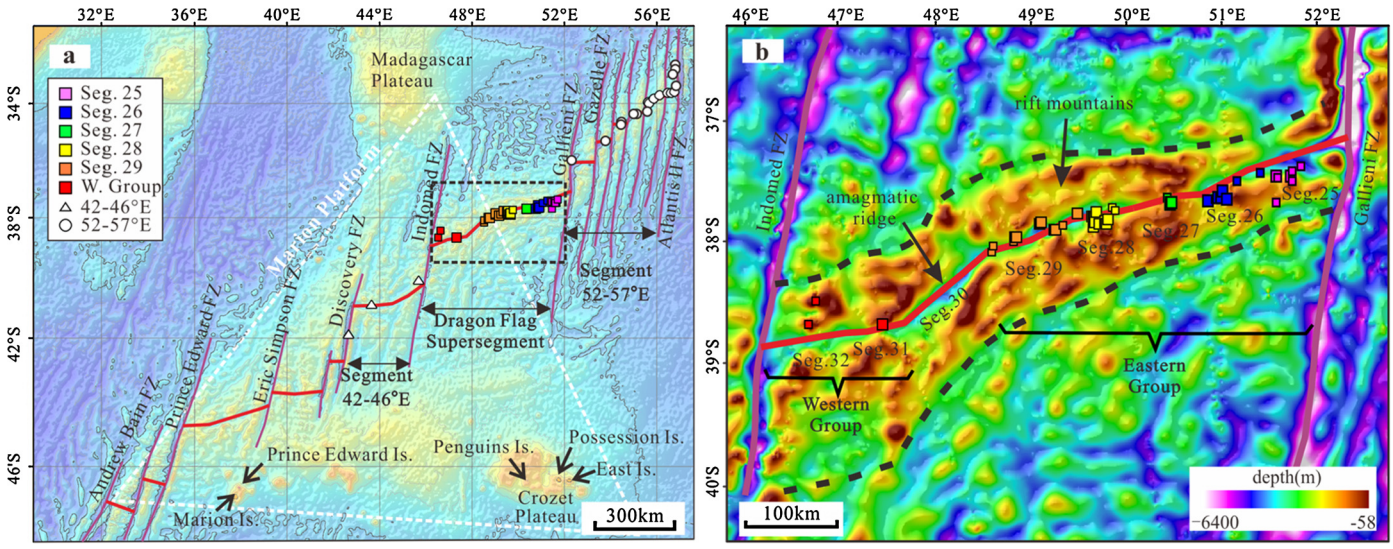

Fig. 1. (a) Bathymetric map for the central part of SWIR with sample locations. Map is contoured every 1,000 m, and −4000 m isobath is highlighted in bold. The white dashed triangle indicates the area of Marion Platform. The black dashed box indicates the location for Fig. 1b. (b) Bathymetry for the Dragon Flag Supersegment with sample locations. Larger symbols of the samples are from this study, while smaller ones are from literature. Individual segments are numbered following and extending the nomenclature of Cannat et al. (1999). The bathymetric data are all from GEBCO. (For interpretation of the colors in the figure(s), the reader is referred to the web version of this article.)

MORB major element compositions. Seismic and gravity observations, however, indicate that this region has the thickest crust yet found along the entire SWIR (Sauter et al., 2009; Niu et al., 2015 and references therein) – a feature usually associated with ridge-hotspot interaction. Sauter et al. (2009) showed that the flanking rift mountains are anomalously 1-2-km higher than adjacent older crust, indicating the sudden onset of excess volcanism beginning at ~8-11 Ma. This volcanism rapidly progressed to the east from the Indomed FZ to Gallieni FZ, creating an eastward narrow v-shaped trend. They also suggested that this was due to interaction with Crozet hotspot 800-900 km to the southeast (Sauter et al., 2009). Breton et al. (2013), based on the Pb-Sr-Nd-He isotopes of the Crozet Archipelagos, also proposed that the upper mantle of the Supersegment was contaminated by the Crozet Mantle Plume. However, the v-shaped bathymetric trend is opposite to that predicted for excess volcanism related to hotspot reference frame, and the propagation rate (~51 mm/yr) exceeds the spreading rate (14 mm/yr) by a factor of 4 – suggesting a plate-controlled source variation for the excess volcanism, rather than a source heterogeneity fixed in the hotspot reference frame. Thus, we present a possible mechanism for local melting anomalies that may be widely, perhaps uniquely, applicable to ultraslow spreading ridges.

Here, we present new major and trace element, and Sr-Nd-Pb isotopic data for the Dragon Flag Supersegment, and review the geochemistry and geology of 5 additional SWIR micro hotspots. This shows their origin is not directly related to the spatially associated Marion and Crozet mantle hotspots. Rather they reflect their plate tectonic setting, with deep regions of melt focusing in the mantle controlled by the lithospheric stress field, interacting with an upper mantle source with components of delaminated ancient continental and arc lithosphere entrained in the asthenosphere.

2. Geological setting

2.1. Regional setting

The SWIR is an ultraslow spreading ridge (~14 mm/yr) that extends a great circle distance of 6,530 km from the Bouvet Triple Junction to the Rodriguez Triple Junction (Fig. 1a). It is dominated by the Marion Rise, an enormous seafloor elevation, which stretches 3,408 km from its deepest point along the ridge west of the Melville FZ (~4,500 m) to the southern ridge-transform intersection of the Andrew Bain FZ (~5,000 m). The rise shoals to a 1.2×10^6 km^2 central region known as the Marion Platform (Dick and Zhou, 2015). The ridge over the platform consists of the eastern 577-km long Dragon Flag Supersegment, a central 305-km saddle, and a 970-km section from the Discovery to Andrew Bain FZ. The eastern and central sections form a spine that bisects a V-shaped bathymetric trend that contains the Marion Hotspot track and the Del Cano Rise. The rise is second only to the Icelandic depth anomaly up the Reykjanes. The Marion Hotspot, has a melt flux only ~6% of the latter, and instead of thick crust, mantle peridotites are exposed on the ridge over the platform, indicating thin and missing crust over large areas (Zhou and Dick, 2013).

The Marion Rise is located over a large negative residual mantle Bouguer anomaly (RMBA), a prominent 4,150,000-km^2 circular 40-m geoid high that encompasses Marion and Crozet Islands, the Del Cano Plateau, and the Conrad Rise. This has been attributed to thick crust due to deep mantle plumes associated with the hotspots (Georgen et al., 2001; Duncan, 1981; Zhang et al., 2011). Alternatively, this anomaly is due to buoyant depleted mantle pulled from beneath the East African-Antarctic Orogenic Belt during Gondwanan breakup of (Dick and Zhou, 2015; Gao et al., 2016; Zhou and Dick, 2013). Consistent with this, Meyzen et al. (2005), based on isotopic evidence, suggest the Marion and Crozet mantle plumes have little influence on the SWIR, while Dalton et al. (2014), using seismic tomography and the MORB composition, find a low mantle potential temperature below it, consistent with them as well.

2.2. The Dragon Flag Supersegment

The 577-km long Dragon Flag Supersegment (46°-52°E) lies between the Indomed and Gallieni FZ's, consisting of eastward north-stepping sub-orthogonal magmatic segments separated by small non-transform discontinuities, and a prominent NE-SW oblique segment between 47°36′ and 48°30′E. Extending the system of Cannat et al. (1999), the segments between 46° and 52°E are numbered 25 to 32 (Fig. 1b). The orthogonal segments are each ~70 km long, while the 124-km long oblique Segment 30 subdivides the Supersegment into western and eastern regions. There are prominent elevated rift-mountains on both flanks, with cross-

Please cite this article in press as: Yu, X., Dick, H.J.B. Plate-driven micro-hotspots and the evolution of the Dragon Flag melting anomaly, Southwest Indian Ridge. Earth Planet. Sci. Lett. (2019), https://doi.org/10.1016/j.epsl.2019.116002

axis relief up to 2 km, and ∼1.7 km excess crustal thickness inferred from gravity compared to older crust to the south and north (Sauter et al., 2009). The shallow ridge flank domains extend up to 75-km's from the rift axis near the Indomed FZ, narrowing to ∼50 km near the Gallieni FZ. The melting anomaly, then, propagated eastward, creating a narrow V-shaped bathymetric trend (Sauter et al., 2009; Zhang et al., 2011). The steep outward boundaries of the shallow domains indicate abruptly enhanced magma supply at ∼11-8 Ma.

Sauter et al. (2009) suggest this magmatism largely died out around 1 Ma. Segment 27, however, has a pronounced axial high filling the rift valley, and seismic data shows there is 9-10 km of crust there (Zhang et al., 2011; Niu et al., 2015), with the crust dramatically thinning to the east and west (Mendel et al., 2003). There is also no neovolcanic zone at either Segment 30 and Segment 25. Segment 27 then is the localized remains of the melting anomaly that created the flanking plateaus.

3. Sample locations and analytical methods

3.1. Sample locations

Cruises DY115-20, DY115-21 and DY125-30 of the *R/V Dayang Yihao* collected basalts within 20 km (or ∼3 Ma) of the ridge axis, from which 30 representative basalts were analyzed for this study. Detailed sample information is in the supplementary material.

3.2. Analytical methods

All analyses were done at the Guangzhou Institute of Geochemistry, CAS. The analytical methods and references are given in the Supplemental Data. Only 2 glass samples were available due to a shortage of glass-encrusted samples. The remaining samples were all fine-grained basalts with limited phenocrysts. Major elements were measured for 30 basalts on fused glass beads by XRF, and trace elements were determined by ICP-MS. Sr, Nd, and Pb isotopes were measured on 19 representative basalts by MC-ICP-MS.

4. Results

4.1. Major elements

Major element compositions for the eastern and western basalts are similar, except for Segment 28, which are more varied (Fig. 2). MgO in most eastern basalts varies from 6.4 to 10 wt.%, while SW28-6 and DY115-19-3-14-2 are higher in MgO (>10 wt.%), and SW28-3 and SW28-1 are lower in MgO (<6.4 wt.%). SW28-6 also has higher CaO, and lower Fe_2O_3t, Na_2O, and TiO_2, consistent with the appearance of olivine and anorthite phenocrysts. Total alkali contents range from ∼1.20 to 4.69 wt.%, and all are low-K tholeiites. Loss on ignition (LOI) is mostly low, <0.65 wt.%, indicating limited alteration. Basalts SW28-13 and SW28-14 have negative LOI values indicating high FeO/Fe_2O_3 ratios. SiO_2, TiO_2 and P_2O_5 increase with decreasing MgO, but no clear correlations exist for other major elements. The Western Group has similar major element compositions, with total alkalis from ∼1.93 to 3.12 wt.%.

4.2. Trace elements

Trace element analyses, with 30 new basalts were screened for quality for a final dataset. Incomplete analyses were excluded as unsuitable for multi-element interpretation. Replicate or excessive data for a station were not used to avoid statistical bias. The basalts were widely distributed, though only 3 are from the west.

Trace element contents in the eastern basalts are relatively homogeneous (Fig. 3). La, for example, is largely restricted to a narrow range (1.44-2.97 ppm), though it is low in SW28-6 (0.39 ppm), and high in SW29-1 and SW29-2 (4.01 ppm and 3.98 ppm). The eastern basalts all have typical REE depleted N-MORB patterns. Chondrite normalized $(La/Sm)_N$ ratios for most are ∼0.37 to 0.57. SW29-1 and SW29-2 have higher $(La/Sm)_N$ ratios (0.61∼0.78), while SW28-6 relatively lower (0.24). Total REE concentrations range from 24 to 78 ppm for most eastern basalts, while SW28-6 has very low REE (15.04 ppm). Europium anomalies are small (0.86-1.20), except one Segment 29 basalt with δEu 0.77 (Font et al., 2007). The eastern basalts are also depleted in Rb, Ba, Th, Nb, Ta, but with some Rb and U spikes due to their great fluid mobility. The western basalts have fairly flat trace element patterns compared to the eastern basalts, with higher $(La/Sm)_N$ ratios (0.74-1.06).

4.3. Sr, Nd and Pb isotopes

Compared to the SWIR to the east and west, the Supersegment basalts have relatively enriched Pb isotopes, though this is less evident for Sr and Nd isotopes (Fig. 4). $^{87}Sr/^{86}Sr$ in the eastern basalts varies from 0.70272 to 0.70361, and $^{143}Nd/^{144}Nd$ from 0.512869 to 0.513181 ($\varepsilon Nd = +4.5 \sim +10.6$), and all but SW28-7, SW28-11 and SW29-3 plot along the mantle array (Fig. 5a). The latter have excess $^{87}Sr/^{86}Sr$ ratios reflecting seawater alteration and are excluded from further discussion. The lowest $^{143}Nd/^{144}Nd$ are in Segment 27 basalts ($\varepsilon Nd = +4.5$), consistent with their high $^{87}Sr/^{86}Sr$. The western and eastern basalts have roughly similar isotopic compositions, the exception of two Segment 31 basalts with lower $^{206}Pb/^{204}Pb$. Most western basalts lie closer to DMM than the remaining Supersegment basalts in Pb-Pb space (Fig. 4), but with lower $^{143}Nd/^{144}Nd$ similar to the enriched Segments 27 and 29 basalts.

5. The Dragon Flag Supersegment: discussion

The origin of the Dragon Flag melting anomaly is of key importance in understanding the magma focusing and extrusion along the SWIR. The mantle source, partial melting process and geodynamic models of the melting anomaly were addressed below.

5.1. Evidence for multiple primary magma

The basalts represent extensive crystal fractionation, with Mg# (Mg∗100/[Mg+Fe]) ranging from ∼52 to 65, with none, excluding SW28-6, close to that expected for a primary magma (72). In Fig. 2 we plot the liquid line of descent (LLD) calculated using Petrolog3 (Danyushevsky and Plechov, 2011) for a reasonable parent magma, compositionally equal to our most primitive basalt. In agreement with Yang et al. (2017), the large scatter about the liquid line of descent for most elements shows that more than one parent magma is required, even for a single segment. Sample SW28-6, in particular, with the lowest and steepest REE pattern (Fig. 3), lowest TiO_2, highest Al_2O_3 and a $Mg^{\#}$ (∼72) in equilibrium with mantle olivine, represents an isotopically unique primary magma (Fig. 5).

5.2. Partial melting modeling

Rare earth and other trace element patterns show differences between the individual Dragon Flag segments (Figs. 3 and 6a), reflecting varying source composition and/or degree of mantle melting. Eastern segment 25, 28 and 29 basalts, excluding 28-6, are virtually identical, with the highest middle rare earths (MREE) and heavy rare earths (HREE), and greatest light rare earth (LREE)

Please cite this article in press as: Yu, X., Dick, H.J.B. Plate-driven micro-hotspots and the evolution of the Dragon Flag melting anomaly, Southwest Indian Ridge. Earth Planet. Sci. Lett. (2019), https://doi.org/10.1016/j.epsl.2019.116002

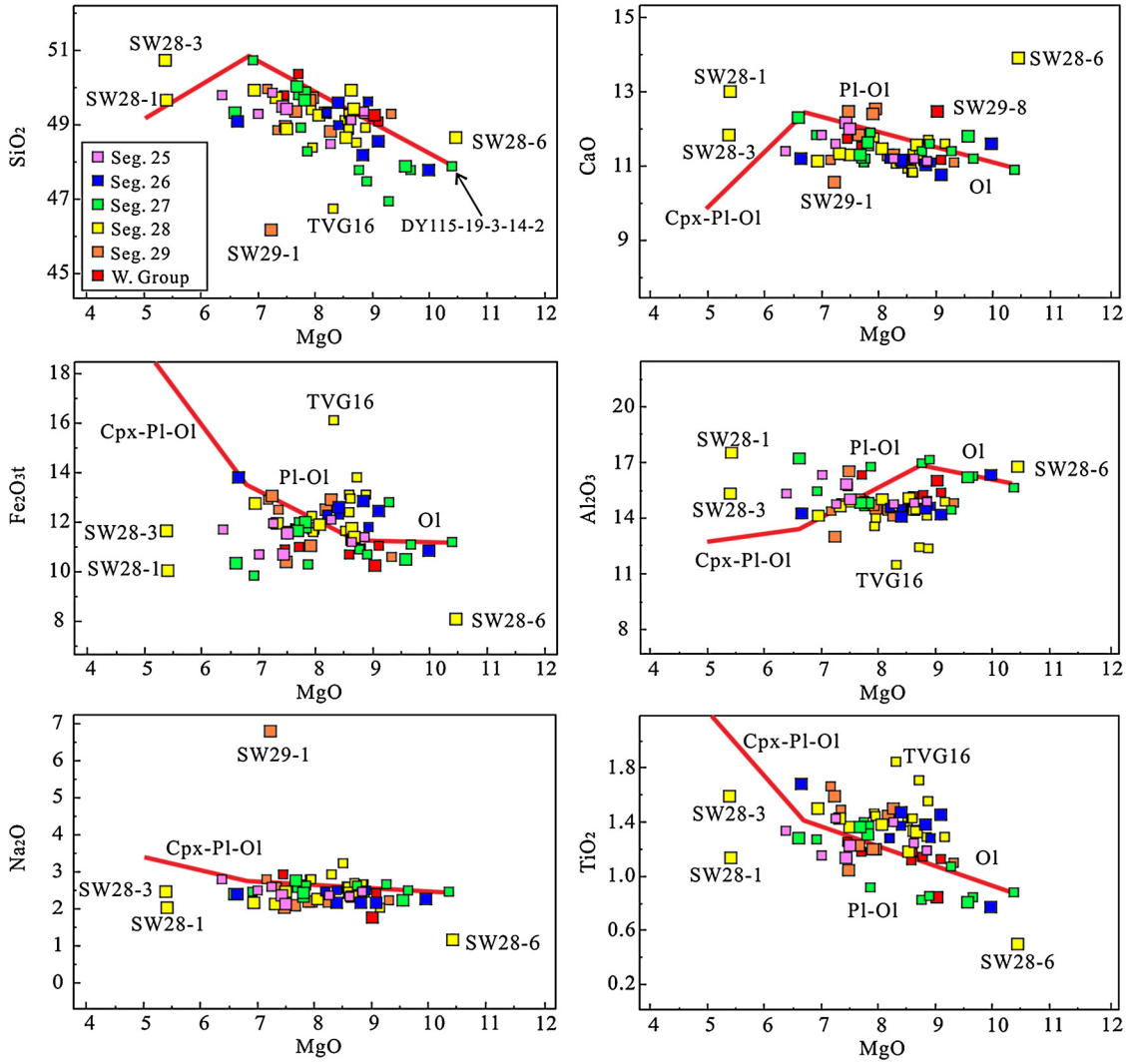

Fig. 2. Major element variations for MORBs from Dragon Flag Supersegment. The liquid line of descent (LLD) has been modeled using the package of Petrolog (Danyushevsky and Plechov, 2011) for a given parental magma. The LLDs shown here (red lines) are the modeling result for a parental magma compositionally similar to basalt DY115-19-3-14-2 (Yang et al., 2017). The initial pressure of the modeling for fractional crystallization is set at 0.33 kbar. The bends correspond to successive fractionation of olivine (Ol), olivine (Ol) + plagioclase (Pl), and olivine (Ol) + plagioclase (Pl) + clinopyroxene (Cpx). The LLD slopes generally change as each new phase appears on the liquidus, except where the successive fractionating assemblage does not significantly fractionate an element (e.g. Ol to Ol + Pl in the lower right TiO_2 vs. MgO plot).

depletion. Segments 26 and 27 are also virtually identical, but less fractionated LREE to HREE, and less LREE depleted compared to segments 25, 28 and 29. The western basalts have the least fractionated REE, with higher $(La/Sm)_N$, than any eastern basalt (Fig. 4a), due either to lower degree partial melting or an initially less depleted mantle source. The outlier Segment 28 basalt SW28-6 has the most depleted pattern with substantially lower total REE's (Fig. 6a).

To constrain basalt genesis, we modeled mantle melting started with DMM. Though the DMM is definitely not the exact mantle source for Dragon Flag segments, assuming a common source in melt modeling is quite helpful to resolve the difference of primary magmas for each segment. As non-modal and modal equilibrium partial melting do not significantly vary melt composition, we use non-modal partial melting for simplicity (Fig. 6b). As the HREE are not depleted compared to the MREE in the Dragon Flag lavas, there is likely little or no garnet in the source.

Based on the modeling, the western basalts (represented by SW31-1) can be generated by 10% partial melting of DMM. The eastern basalts, however, require multi-stage partial melting due to their depleted LREE signatures (Fig. 6c). If DMM is the original source, then two-stage melting is required to explain the Eastern Group REE. Remelting of previously depleted mantle can generate the LREE-depletion. Ignoring mantle heterogeneity, 1% remelting of the residue after 10% first-stage melting would produce the parent magma for segments 26 and 27, while ~5% can generate the more depleted segment 25, 28 and 29 basalts (Fig. 6d). We note that given the ~9-km thickness of the Segment 27 crust, that this model predicts more like ~4-km of crust. Thus, a more realistic model would require a significantly more fertile bulk source composition, likely a multi-component mix of pyroxenite veins and a DMM-like host. However, this shows that whatever the mantle composition is, the REE patterns can be explained by a two-stage melting model.

5.3. The supersegment mantle source

Several authors attribute the Dragon Flag magmatism to interaction with a deep mantle plume associated with the Crozet hotspot 800-900 km to the south (Sauter et al., 2009; Breton et al., 2013; Yang et al., 2017). The V-shaped trend, however, is opposite to that predicted for excess volcanism related to the hotspot ref-

Please cite this article in press as: Yu, X., Dick, H.J.B. Plate-driven micro-hotspots and the evolution of the Dragon Flag melting anomaly, Southwest Indian Ridge. Earth Planet. Sci. Lett. (2019), https://doi.org/10.1016/j.epsl.2019.116002

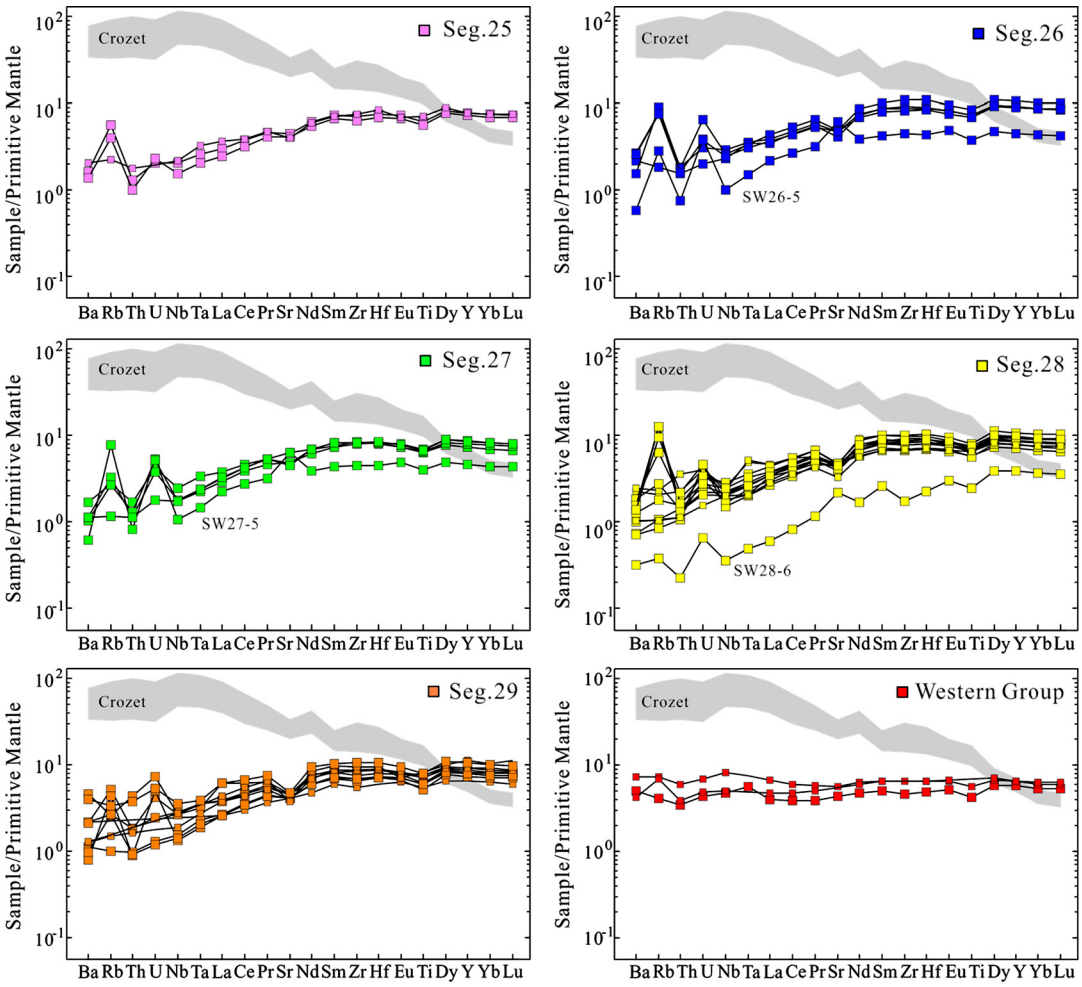

Fig. 3. Primitive mantle-normalized multi-element patterns of basalts from each segment of Supersegment. Normalization values follow Sun and McDonough (1989). Shaded field is the reference of ocean island basalts from Crozet Archipelagos (Breton et al., 2013). The large variation of Rb and U compositions could be due to their greater fluid mobility.

erence frame, and the propagation rate (~51 mm/yr) exceeds the spreading rate (14 mm/yr) by a factor of 4 – suggesting a plate-controlled source variation for the excess volcanism.

In terms of Sr and Nd isotopes most basalts had a depleted mantle source with positive εNd (Fig. 5). There are enriched basalts with higher $^{87}Sr/^{86}Sr$ and lower εNd at two Segment 27 locations (Yang et al., 2017), and one segment 29 basalt (SW29-1; Fig. 4). Pb isotope enrichment is more evident, especially for the Eastern Group. Both eastern and western suites have high $^{207}Pb/^{204}Pb$ ratios at a given $^{206}Pb/^{204}Pb$ characteristic of the Indian Ocean DUPAL anomaly (Hart, 1984). Though, it seems the Sr-Nd isotopes and $^{208}Pb/^{204}Pb$ versus $^{206}Pb/^{204}Pb$ can be explained by simple mixing of DMM and Crozet (Fig. 5), in the $^{207}Pb/^{204}Pb$ - $^{206}Pb/^{204}Pb$ plot they point not to Crozet but to EMII, which is akin to Madagascan lavas (Fig. 5c). The Sr-Nd isotopic variations also support the mixing between EMII-like component and DMM. Thus, it is hard to explain the isotope systematics by mixing Crozet and DMM sources.

A 3-component mixing model can explain the isotopes using DMM, an EMII-like enriched source and a Madagascar-like component (Fig. 5c). DMM is the main component of the Supersegment source, which would be low $^{87}Sr/^{86}Sr$, high $^{143}Nd/^{144}Nd$ and low Pb isotopes. The Madagascar-like component could explain the DUPAL anomaly. The contribution of enriched EMII-like material, which could be Crozet-like in this model, and elevate the Pb isotopes.

Alternatively, a pseudo-binary mixing of DMM and an enriched component could be used. However, this component cannot be only Crozet, as suggested by Yang et al. (2017), as it deviates from it in $^{207}Pb/^{204}Pb$ - $^{206}Pb/^{204}Pb$ space. The enriched component is geochemically equivalent to a mixture of EMII- and Madagascar-like material, which could be continental crust or subcontinental lithosphere mantle (SCLM). This can explain the higher $^{87}Sr/^{86}Sr$, and more radiogenic Pb isotopes, and is consistent with physically mixing the EMII- and Madagascar-like components before adding it to DMM. This is supported by Madagascar tholeiites contaminated by sub-continental lithospheric mantle during eruption (Mahoney et al., 1991).

The shallow depth and thickened crust of the Dragon Flag Supersegment is a characteristic of ocean rises near hotspots. Thus, Sauter et al. (2009) proposed this was the result of interaction with a mantle plume associated with the Crozet Archipelago. Breton et al. (2013) show that the Dragon Flag basalt isotopic compositions can be modeled as a mixture of DMM with Crozet and FOZO source components. Yang et al. (2017) proposed that during upslope flow of a Crozet mantle plume to the ridge, decompression melting along the path, would deplete the plume in incompatible elements, but not significantly change its isotopic composition. Remelting this residue by further melting beneath the ridge would then produce isotopically enriched N-MORB at Segment 27. Such models, though they can successfully reproduce characteristics of the Supersegment basalts, are geologically unrealistic. Moreover,

Please cite this article in press as: Yu, X., Dick, H.J.B. Plate-driven micro-hotspots and the evolution of the Dragon Flag melting anomaly, Southwest Indian Ridge. Earth Planet. Sci. Lett. (2019), https://doi.org/10.1016/j.epsl.2019.116002

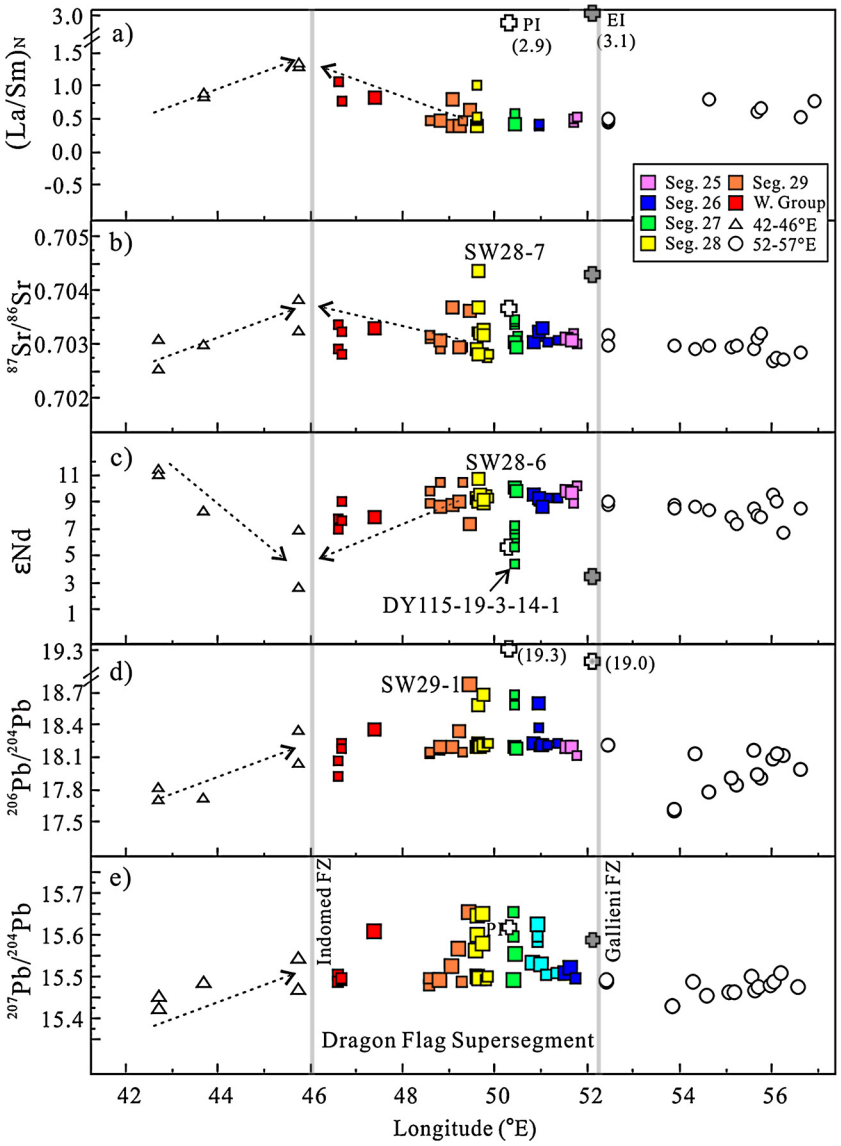

Fig. 4. (a-e) Along ridge variations of $(La/Sm)_N$, $^{87}Sr/^{86}Sr$, εNd, $^{206}Pb/^{204}Pb$, and $^{207}Pb/^{204}Pb$ for MORBs from the Supersegment and adjacent ridge segments. $(La/Sm)_N$ represent the normalized La/Sm ratios by primitive mantle according to Sun and McDonough (1989). Samples PROT-5-37-1 and PROT-5-37-3 from le Roex et al. (1989) are out of the range in Fig. 4a. Also shown are the average $(La/Sm)_N$ and isotopic compositions of Crozet Hotspot basalts, from Penguins Island (PI) and East Island (EI, including Possession island). Data for Crozet archipelagos are from Breton et al. (2013).

though a Crozet component can be used arbitrarily in the three-component mixing model, an infinite number of other components would be equally applicable (e.g.: Marion), and equally unlikely geologically.

Many authors, however, have found that the large differences in isotopic composition between the Crozet and Dragon Flag basalts are inconsistent with any direct interaction (e.g.: Mahoney et al., 1992; Meyzen et al., 2005). The $^{207}Pb/^{204}Pb$ ratios for some portions of segments 27, 28, and 29 are even higher than that for Crozet hotspot, thus it is impossible to explain by a mixing process. Yang et al. (2017) also found a Crozet influence only for Segment 27. It is hard to explain, then, why this is not seen at Segments 28 and 29. The small-scale heterogeneity within a segment is also difficult to explain by plume-ridge interaction (e.g. Segments 27 and 28). Based on plate reconstruction, the Crozet hotspot is currently beneath crust formed at the SE Indian Ridge, rather than at the SWIR (Zhang et al., 2011), and thus the LAB slopes in the wrong direction. It also lies south of the NE extension of the Del Cano Rise, whose thickened lithosphere would likely impede mantle flow from Crozet to the ridge. Most telling, the Crozet archipelago, though volcanically active, has no hotspot track, indicating it does not represent a classic deep mantle plume. Moreover, while seismic crustal thickness has been measured up to 10.2 km at Segment 27 (e.g., Niu et al., 2015), it rapidly thins to the west, and virtually disappears 80-km east. Thus, overwhelming geological, geophysical and geochemical evidence suggests Crozet has no direct relationship to the Dragon Flag Supersegment.

Mixing models, however, are best used when constrained by the plate tectonic setting. The enriched component for Dragon Flag basalts can be continental crust, or oceanic crust, including sediments (Dupré and Allègre, 1983; Rehkämper and Hofmann, 1997; Meyzen et al., 2005; Gautheron et al., 2015, and references therein) sheared off from the Gondwanan lithosphere during breakup and formation of the SWIR. SCLM could also be eroded into the asthenosphere due to the mantle plume associated with the Karoo basalts, supplying the Marion Platform and Supersegment enriched component (e.g.: Mahoney et al., 1992). Tectonically, Madagascar and the Madagascar Plateau used to be part of East Africa-Antarctic

Please cite this article in press as: Yu, X., Dick, H.J.B. Plate-driven micro-hotspots and the evolution of the Dragon Flag melting anomaly, Southwest Indian Ridge. Earth Planet. Sci. Lett. (2019), https://doi.org/10.1016/j.epsl.2019.116002

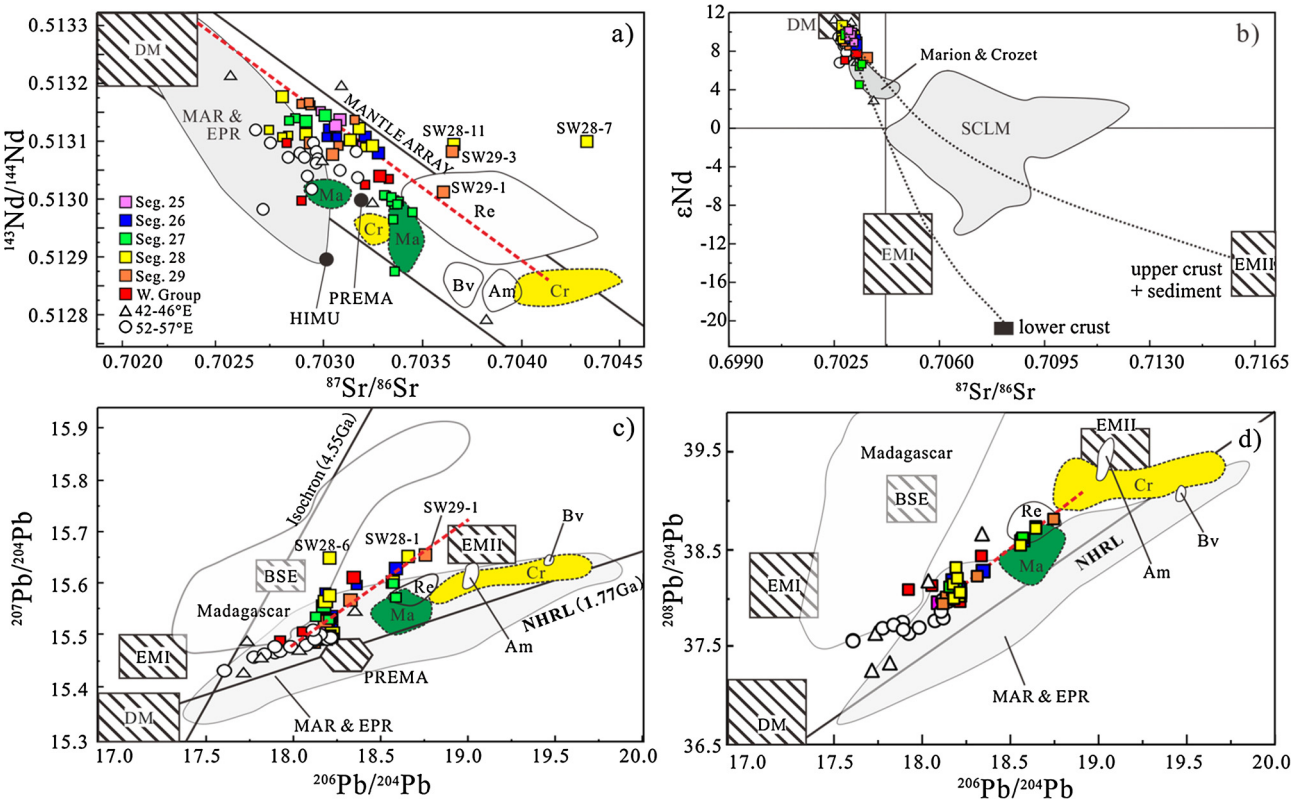

Fig. 5. (a) and (b) $^{143}Nd/^{144}Nd$ vs. $^{87}Sr/^{86}Sr$, (c) $^{207}Pb/^{204}Pb$ and (d) $^{208}Pb/^{204}Pb$ vs. $^{206}Pb/^{204}Pb$ variations for MORBs from Dragon Flag Supersegment and adjacent ridge segments. Also included are those isotopic data for Crozet (Cr), Marion (Ma), Bouvet (Bv), Amsterdam (Am), Reunion (Re) and Madagascan (Mad) lavas. The data sources for Amsterdam, Bouvet, Marion, Crozet, Reunion and Madagascan lavas are from Doucet et al. (2004), Janney et al. (2005), le Roex et al. (2012), Breton et al. (2013), Mahoney et al. (1989) and Mahoney et al. (1991), respectively. The data for Mid-Atlantic Ridge (MAR) and East Pacific Rise (EPR) are from PetDB. The cross-hatched box indicates the mantle endmembers (DM, EMI, EMII, PREMA, BSE) suggested by Zindler and Hart (1986). The data source for SCLM in Fig. 5b is from Hawkesworth et al. (1990), the sediment from Rehkämper and Hofmann (1997), the upper crust from Miller et al. (1999), the lower crust from Ben Othman et al. (1984). The dashed red line represents the dominant trend of the supersegment data.

Orogenic Belt (Stern, 1994), and the central part of SWIR, including the Supersegment lies directly to the south. Thus, the source of the melting anomaly could be delaminated or sheared off ancient continental lithospheric fragments from that orogenic belt. This would include old depleted supra subduction zone mantle with entrained subducted Archean and Neoproterozoic sediments, and old Mozambique Ocean crust, and numerous Neoproterozoic arc and back-arc lithospheric fragments including metasomatized older Archean lithosphere (e.g.: Collins and Windley, 2002). This witch's brew of isotopic sources is consistent with the diversity found on the Marion Platform, including Marion and Crozet. So, Crozet likely also formed as a result of melting of an enriched component foundered in the asthenosphere during Gondwanan breakup, just as we propose the Supersegment did, which explains any geochemical affinity between them and the absence of a Crozet hotspot track. We note, however, that some Crozet basalts have high $^{3}He/^{4}He$ (Breton et al., 2013), which is consistent with slightly high $^{3}He/^{4}He$ in the Dragon Flag basalts, which indicates that other components than those derived from the delaminated old continental lithosphere are involved in their genesis.

5.4. Geodynamic model of the Dragon Flag melting anomaly

The Dragon Flag melting anomaly propagated rapidly east, independent of the hotspot reference frame at a velocity almost 4 times the spreading rate; faster than any known hotspot track. Ridge-segment migration, however, has been widely documented at ocean ridges due to far-field plate forces, in response to spreading direction changes, local variations in the stress field, and to enhanced or reduced melt flux at individual segments. We propose then that the sudden influx of melt followed a major change in the source composition drawn into the melting column at ~11-8 Ma. This triggered a local plate reorganization, with the segment overlying the greatest melt flux migrating rapidly to the east, with an enhanced melt flux in the trailing segments as well, which has now localized to Segment 27.

Segment 30 has a trailing oblique segment morphologically similar to those trailing our point source micro hotspots discussed below, followed by two magmatic segments with a deep rift valley, indicating a sharp reduction in melt supply as the melting anomaly receded to the east. Consistent with this, Segment 32 has higher Na_8 than Segment 31, while the eastern basalts are even lower (Fig. 7). This indicates a systematically more refractory source or progressively higher degrees of mantle melting from west to east (Dick and Zhou, 2015), as also indicated by the trace element modeling. The Segment 31 basalt has more enriched Pb isotopes and lies at the high end of the Segment 32 basalts, while the eastern basalts have significantly more radiogenic lead, and extend to even higher $^{87}Sr/^{86}Sr$ (Fig. 4). For this to happen requires the eastern mantle source to be more enriched in the low-temperature melting component.

The enormous crustal thickness at Segment 27, is inconsistent with a more refractory mantle source, indicating that the basalts are products of a high-degree mantle melting. The Na_8 of 2.41 wt.%, though, implies a crustal thickness of only ~4 km following Klein and Langmuir (1987), while their correlation with depth predicts a Na_8 of ~2.0 for 10-km thick crust. However, the more radiogenic isotopic composition of the lavas also indicates a change

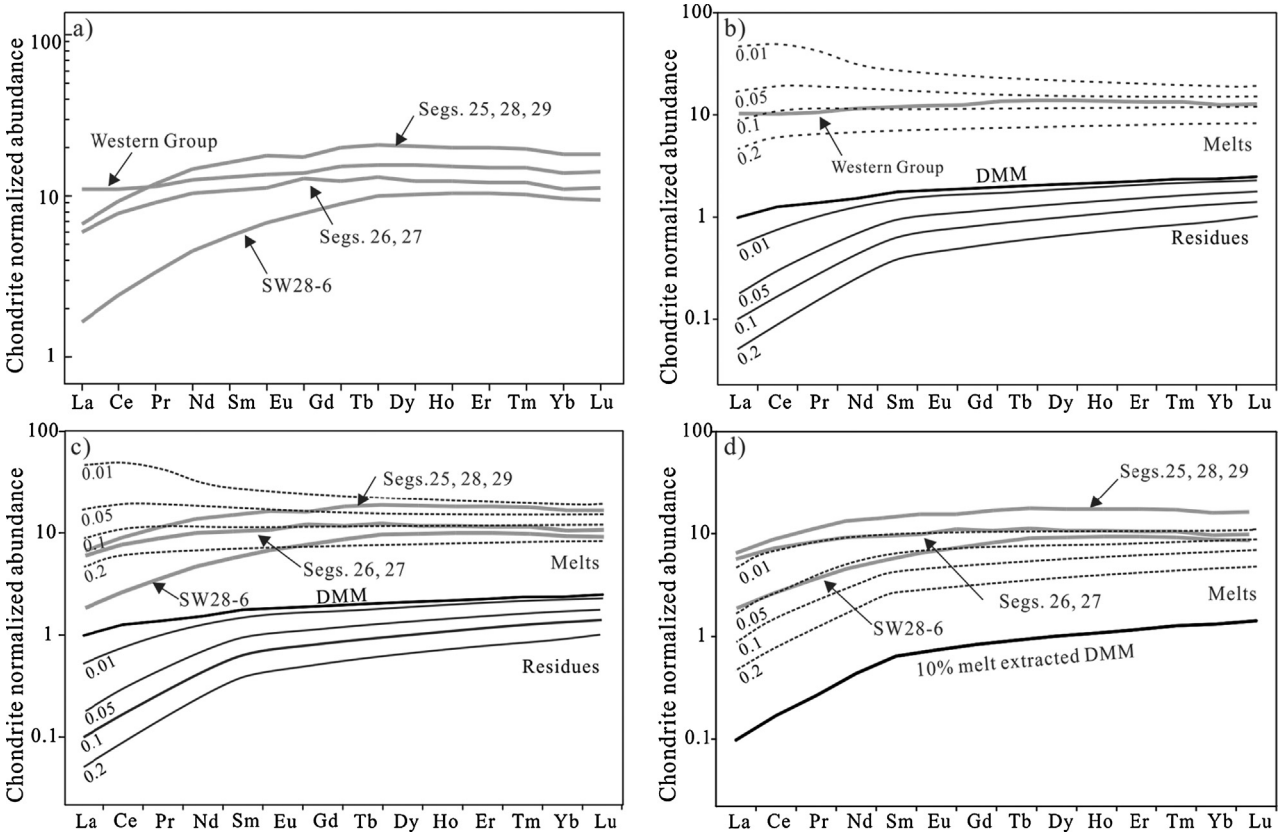

Fig. 6. (a) The REE patterns for representative samples from each segment. (b) and (c) Non-modal equilibrium partial melting result for a depleted mantle source (DMM) compared with selected typical basalts from the Western Group and the Eastern Group, respectively. (d) Remelting of a mantle residue which had experienced earlier 10% melting and melt extraction. Thin dashed lines represent equilibrium melt compositions, while thin solid black lines represent their respective residues. Annotated numbers represent melt fraction removed from the residues. The detailed parameters chosen for the modeling are listed in Appendix B.

in the proportion of an isotopically enriched relatively fertile component embedded in the otherwise very depleted asthenosphere of the Marion Platform, where the residual peridotites are generally low-alumina pyroxene-poor harzburgites (e.g.: Gao et al., 2016). The fluxing effect of the increased alkalis, and possibly water, in a significantly increased proportion of enriched component on the regionally depleted mantle could account for the amount melt produced without requiring a very large thermal anomaly, while still producing an anomalously soda-rich melt.

6. Isolated SWIR micro hotspots

Apart from the micro hotspot now centered at segment 27 of SWIR, there are more analogues that can be identified along the ridge, such as Joseph Mayes Seamount, Narrowgate Segment, SWIR 16°E Segment, and the Eastern SWIR 60°-70°E.

6.1. Joseph Mayes Seamount

Joseph Mayes Smt is an enormous sigmoidal 1.36 Ma old axial volcano at 11.3°E that formed in, and replaced an oblique amagmatic spreading center. It connects to a 14-km long incipient transform on the west and an 80-km long oblique-amagmatic spreading center on the east (Fig. 8a). The volcano is 2.6-km high, 28-km wide, and 56-km long and has a 9-km wide 784-m deep axial graben flanked by walls that shoal to 1,000 m. The floor of the graben at 1,673-m depth is one of the shallowest on the SWIR despite the great depth of the SWIR in this region.

Mayes Smt erupts mostly alkali basalt (0.16-1.08 wt.% K_2O), though it is far from any mantle hotspot, with 3.25 average Na_8, and Fe_8 from 7.32 to 9.72. Isotopically, the basalt lies close to EMII along a $^{208}Pb/^{204}Pb$-$^{206}Pb/^{204}Pb$ mixing line with DMM, but has significantly less radiogenic Sr than the central and eastern SWIR basalts (Fig. 7). It is significantly more depleted, however, than either Bouvet Island to the west or the Narrowgate Segment to the east. This unusual volcanism, far from any hotspot, is explained by highly focused melt delivery, with an exceptionally broad zone of melt contribution combined (Fig. 8d) due to an unusually thick lithospheric lid that limits mantle melting so that magmas largely consist of an isotopically enriched low-melting point component (Standish et al., 2008).

6.2. Narrowgate segment

From 9° to 16°E there is a 400-km long oblique supersegment oriented at a steep angle to the spreading direction consisting of four sub-orthogonal magmatic segments, including Joseph Mayes Smt at 11.3°, 12.9°, Narrowgate at 14.7°, and the 16°E segment, 57, 12, 40, and 48-km long respectively (Fig. 8b). They are linked by three amagmatic accretionary segments 80, 94, and 62-km long, oriented up to 32° from the spreading direction (Fig. 8c). The Narrowgate and 16°E segments, have left long oblique traces of anomalously elevated axis-parallel lineated volcanic crust in the southern rift mountains. Each is flanked on the west by a trailing amagmatic segment, and a triangular mantle region that spread directly to the seafloor. Spreading was highly asymmetric to the southeast, accounting in good part for the strong topographic asymmetry north and south of the ridge.

Narrowgate, which gets its name from its narrow 15-km wide 2-km deep rift valley, began its eastward migration at ~3-4 Ma at 16 mm/yr, exceeding the spreading rate. Although it has a much deeper rift valley, greater age, and long trace in the rift mountains,

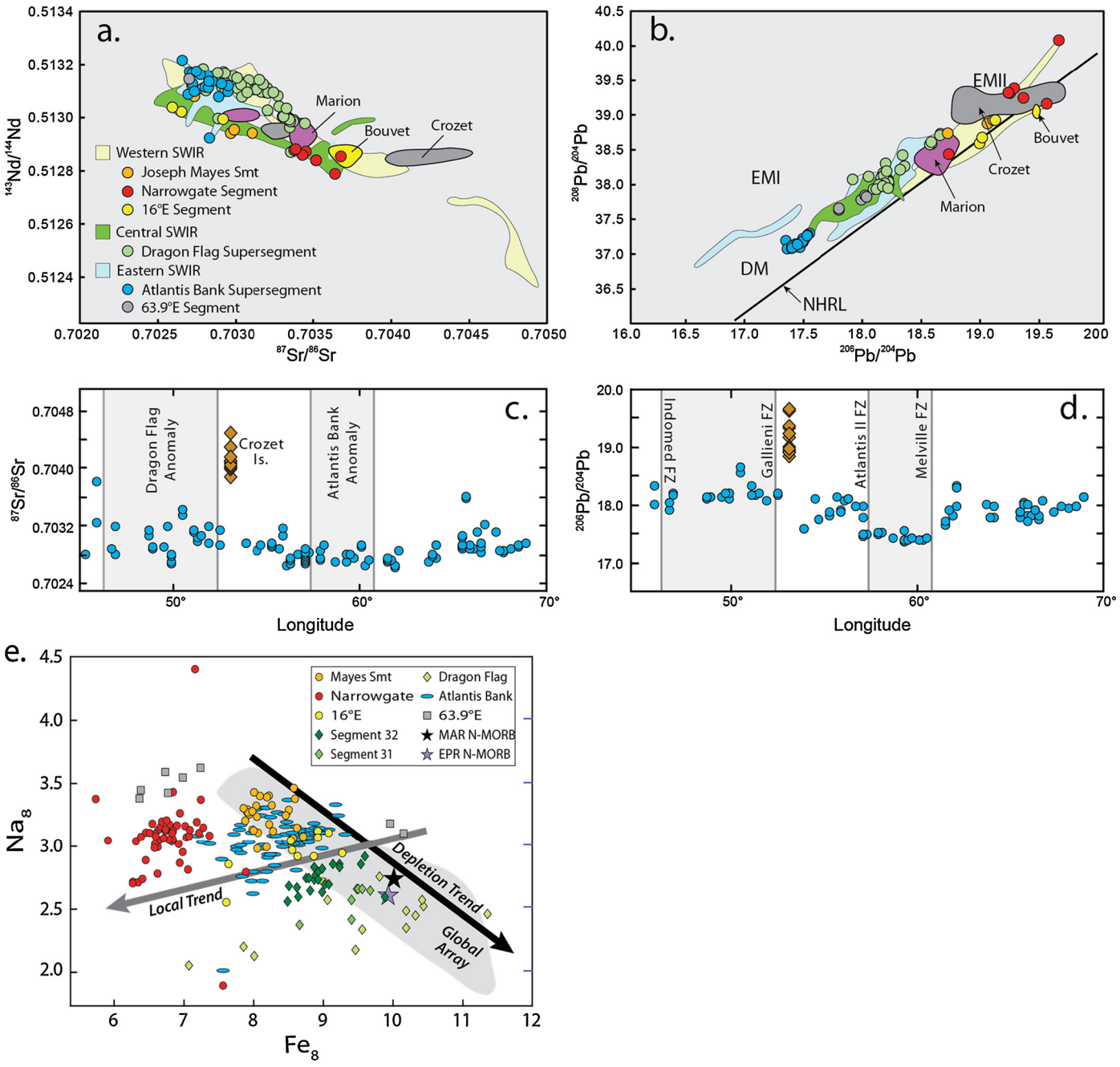

Fig. 7. SW Indian Ridge micro hotspots basalt compositions. (a) Nd and Sr isotopic data, and (b) lead isotopic data for SWIR micro hotspots. Fields for mantle hotspots and SWIR are shown as labeled on the figure. Fields for SW Indian Ridge, are Bouvet Triple Junction to Andrew Bain FZ (western), Andrew Bain to the Gallieni FZ (central), Gallieni to Rodriguez Triple Junction (eastern). Marion, Bouvet, and Crozet and SWIR fields from PetDB, Joseph Mayes Seamount and Narrowgate Segment from Standish (2006) and Mahoney et al. (1992). (c) and (d) SWIR and Crozet Island isotopic compositions versus longitude: mid-ocean ridge basalt – filled blue circles; Crozet Island basalts – brown diamonds. Data from Mahoney et al. (1989, 1992); Snow (1993) and EarthChem/PetDB. Fracture zone locations are indicated by the grey lines. Grey shaded fields indicate the Dragon Flag and Atlantis Bank Melting Anomalies. (e) Weight percent sodium and iron corrected for fractionation to 8 wt.% MgO following Klein and Langmuir (1987) for micro-hotspot basalts. Data from PetDB, Standish et al. (2008), and this paper (Dragon Flag Segment). Grey field is the global ridge array from Klein and Langmuir (1987).

its sigmoidal shape is essentially identical to Mayes Smt. It has a 546-m high axial neovolcanic zone, while the rift valley floor lies at 3,200-m depth compared to 1,673 m for Maye Smt. Though the neovolcanic zone is much deeper than at Mayes Smt, there is also recent volcanism at the crest of its northern rift valley wall (Standish and Sims, 2010). Narrowgate is presently erupting isotopically enriched alkali basalt ($^{87}Sr/^{86}Sr$ from 0.7034 to 0.7036) very similar to Bouvet Is basalt in the rift valley and at the rift mountain volcano (Fig. 7) (le Roex et al., 1992; Standish, 2006).

6.3. SWIR 16°E segment

The 16°E segment has greater relief than Narrowgate, and migrated faster to the east, linking to a magmatic segment across a small discontinuity (Fig. 8b). In this region the SWIR has substantially less ridge obliquity, and therefore significant faster mantle upwelling. 16°E is also isotopically more depleted than Narrowgate (Fig. 7), but similar to Mayes Smt. The basalts are high potassium tholeiites with 0.37 K_2O (Table 1).

Please cite this article in press as: Yu, X., Dick, H.J.B. Plate-driven micro-hotspots and the evolution of the Dragon Flag melting anomaly, Southwest Indian Ridge. Earth Planet. Sci. Lett. (2019), https://doi.org/10.1016/j.epsl.2019.116002

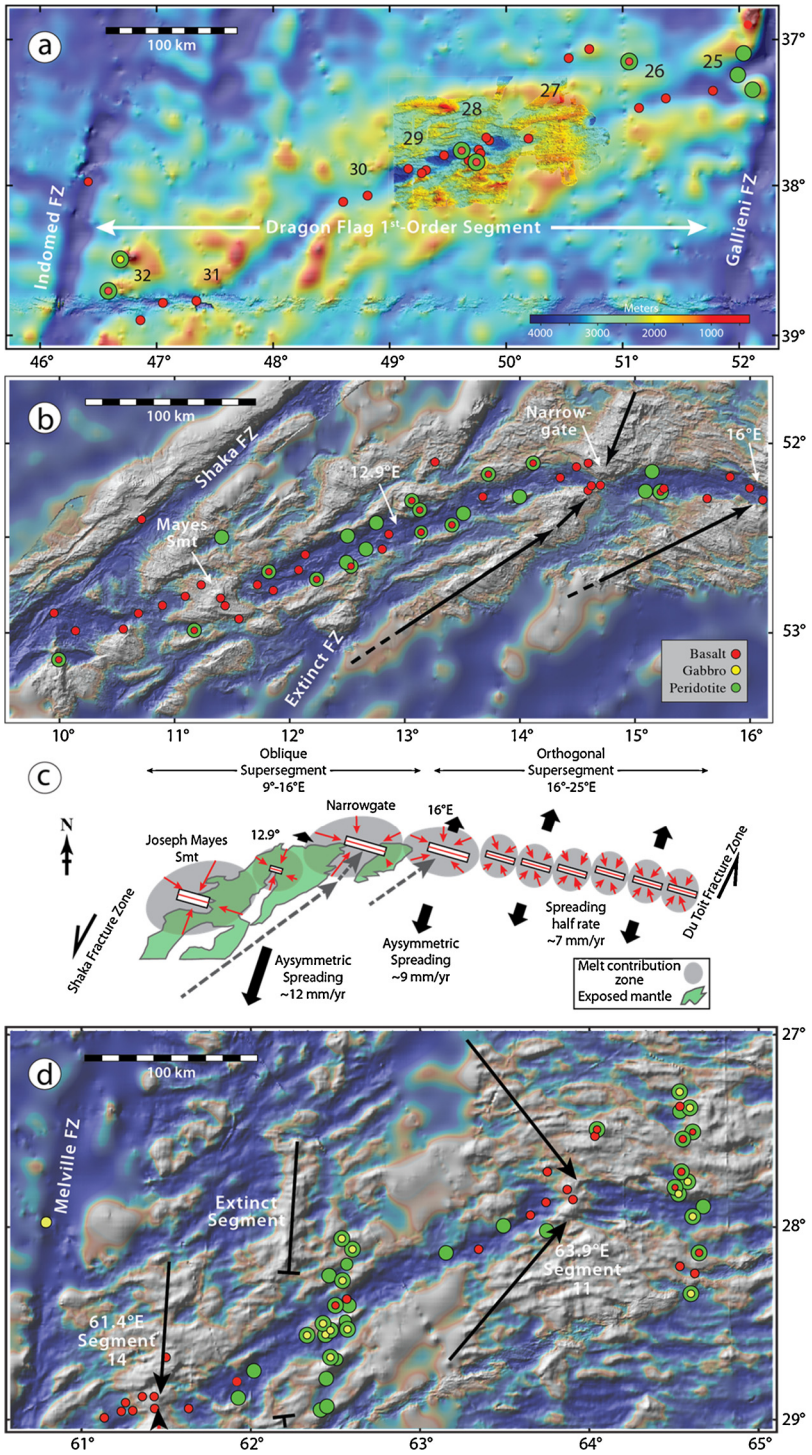

Fig. 8. Shaded relief map of (a) Dragon Flag Supersegment satellite-derived bathymetry with sea surface bathymetry, (b) 9° to 16°E oblique spreading center and Joseph Mayes Smt and the Narrowgate Magmatic Segment. (c) Cartoon showing the Narrowgate and 16°E micro-hotspot traces. Green shaded region shows mantle exposed by amagmatic spreading during magmatic segment migration. Underlying grey areas and red arrows show the hypothetical melt contribution zones beneath individual ridge segments modified from Standish et al. (2008). Heavy black arrows show the extreme spreading asymmetry to the south during Narrowgate and 16°E Segments northeast migration. (d) 61.4° and 63.9°E Micro Hotspots. Long black arrows in (a-d) indicate the traces of micro-hotspots.

6.4. Eastern SWIR 60°-70°E

From 60° and 70°E are a series of exceptionally widely-spaced large magmatic centers separated by amagmatic ridge segments (Sauter et al., 2013). The active volcanoes are typically 40-60 km long and ~3 km high, with flanking 5-km deep oblique spreading centers. Rommevaux-Jestin et al. (1997) attributed them to a thick lithospheric lid, wide spacing, and extreme melt focusing. They have created cross-axis highs or plateaus that extend into the rift mountains from 105 to 133 km with 1-2 km of excess relief (Fig. 8d). The volcanic center at 62°12′E, however, is extinct, and the plateau is split by a 5.2 km deep, 60-km wide rift valley. These volcanic centers then, are ephemeral, likely existing for up to 20 Myr, then dying out with volcanism shifting elsewhere.

The volcanic segment at 63.9°E is very similar to the Narrowgate Segment (cf. Figs. 7b and 7d), having migrated 90 km to the

Please cite this article in press as: Yu, X., Dick, H.J.B. Plate-driven micro-hotspots and the evolution of the Dragon Flag melting anomaly, Southwest Indian Ridge. Earth Planet. Sci. Lett. (2019), https://doi.org/10.1016/j.epsl.2019.116002

Table 1
SW Indian Ridge micro hotspot lavas.

	Longitude	Mg#	sd	K_2O	sd	N	Na_8	sd	Fe_8	sd	N
Joseph Mayes	10.84-11.72	55.5	7.2	0.53	0.26	51	3.25	0.33	7.56	0.69	45
Narrowgate	14.42-14.92	58.3	5.13	1.26	0.21	85	2.96	0.34	5.57	0.53	79
16°E	15.86-16.30	59.9	2.4	0.37	0.08	12	3.01	0.12	8.79	0.75	14
Dragon Flag	46.18-52.22	57.8	2.45	0.15	0.06	63	2.58	0.21	9.40	0.89	49
Western group	46.18-47.72	57.8	0.99	0.17	0.04	29	2.70	0.12	9.07	0.38	29
Eastern group	48.47-52.22	57.7	3.23	0.12	0.07	34	2.41	0.20	9.87	1.19	20
Segment 27	49.91-50.83	59.85	3.3	0.13	0.05	9	2.43	0.22	9.45	1.46	5
Atlantis. Bank	57.08-60.72	54.9	3.2	0.26	0.04	88	3.10	0.22	8.41	0.58	87
Segment 17	58.44-58.85	62.3	-	0.04	-	1	3.31	-	8.72	-	1
Segment 11 (63.9°E)	63.62-64.21	62.3	3.48	0.19	0.09	13	3.77	0.13	7.81	1.58	13
Average SWIR	0.01-70.32	58.2	6.5	0.34	0.33	1420	3.10	0.48	8.34	1.3	1206

Note that grey shading indicates a point-source micro-hotspot, while unshaded indicates large multi-segment anomalies. Mg# = 100∗Mg/(Mg+Fe^{total}), sd = 1 standard deviation, N = number of samples.

ENE at ~7 mm/yr, leaving a long deep trailing amagmatic rift 61° oblique to spreading direction. While the rift valley floors to the east and west average over 5,000-m deep, the axial volcano peaks at 2,261 m below the sea level, and has a 1,617 m cross-axis high lying in a 30-km wide rift valley. The 63.9°E basalts have the highest average Na_8 (3.77), high Fe_8 (7.81) and lowest K_2O (0.19) of any of our micro hotspots. They are also strongly depleted in HREE and elevated LREE (Meyzen et al., 2005) consistent with extensive melting in the garnet stability field. Isotopically they are depleted MORB with low $^{87}Sr/^{86}Sr$ (0.7026-0.7032) and high $^{143}Nd/^{144}Nd$ (Fig. 7).

6.5. Segment scale micro hotspots — discussion

The micro hotspots all have anomalously large volcanic edifices and thickened crust compared to the rest of the SWIR, where the crust is often thin, or even missing. All represent plate-driven segment migration, and adjustment to an evolving lithospheric stress field, and thus sample the ambient regional mantle composition. The question is, are they the result of higher mantle potential temperature, compositional heterogeneity, or melt focusing? The relatively short length scale combined with the long duration of the melting anomalies should rule out thermal anomalies. Thus, we consider extreme melt focusing and mantle source heterogeneity, fertility and degree of melting to explain their origin.

Mayes Smt, Narrowgate, 16°E, and 63.9°E all represent point source volcanoes adjacent to oblique amagmatic segments. Overall, all four localities lie at the upper end of the global Na_8-Fe_8 array of Klein and Langmuir (1987), and this conventionally implies colder mantle melting at shallower depth, resulting in low extents of melting and/or a more fertile source composition (Dick and Zhou, 2015). Higher Fe_8 could be expected due to the thick lithospheric cap at a highly oblique ultraslow spreading ridge, which should result in higher mean pressure of melting. It is only when average Na_8-Fe_8 compositions for individual localities are plotted that a coherent global trend of decreasing Na_8 with increasing Fe_8 appears. This trend can reflect either an increasing degree of melting of a common mantle source, and/or an increasingly refractory mantle source composition (Dick and Zhou, 2015). However, plotted individually, basalt Na_8-Fe_8 lie along trends orthogonal to the global trend defined by average compositions with half the data plotting to the left of the global trend. This enrichment in Fe_8, and slight decrease in Na_8 is generally attributed to melt-rock reaction during melt migration through the lithosphere (Dick and Zhou, 2015, and references therein). The extreme shift of the data for Narrowgate outside the global array may also be due to the effects of their high water and alkali contents in these basalts (Narrowgate: 0.44-1.04, Joseph Mayes Smt 0.54-0.77, and 16°E 0.36 to 0.40 wt.% H_2O, (Standish et al., 2008)). Thus, interpreting Fe_8 as reflecting a mean depth of melting should be done with caution at best. The large spread in our data for the 4 segment-scale micro hotspots, however, is consistent with melt rock reaction during transport through the undulating ≥30-km thick brittle lithosphere found beneath the oblique segment (Schlindwein and Schmid, 2016). This is due to the excess heat loss by conductive cooling at ultraslow effective spreading rates (ESR) corrected for slowing of mantle upwelling due to oblique spreading (Dick et al., 2003).

Due to ridge obliquity, the ESR for Mayes Smt is 3.9 mm/yr which would increase progressively to a rate of 6.2 mm/yr at 16°E, and thus the influence of the lithosphere on the melt composition due to reactive crystallization should progressively decrease from Mayes Smt to 16°E. However, this is complicated by considering that the underlying plumbing systems beneath these volcanic centers may reflect their very different physiographies as well.

Notably only Mayes Smt and the 16°E Segment bear any isotopic similarity, with overlapping ranges of heavy isotopes lying close to EMII. Mayes Smt, however, has significantly higher K_2O and Na_8 and lower Fe_8 than 16°E, suggesting its higher K_2O reflects shallower and lower degree melting of a similar source followed by enrichment in K_2O during additional fractional crystallization consistent with its lower Mg# (55.5 vs 59.9, Table 1). The higher Fe_8, lower K_2O, and MORB-like chemistry, all suggest a higher degree and greater mean depth of mantle melting at 16°E than either Mayes Smt or Narrowgate (Table 1). While the closer ridge segment spacing, indicates that the underlying zone of mantle melt contribution is smaller than for Narrowgate (Fig. 8c), would be compensated for by faster mantle upwelling due to its higher ESR, thinner lithosphere, and a shallower mean depth of melting. This changes the relative contributions of the different components in the mantle source, however, diluting the enriched component, as the more refractory depleted component melts more extensively at 16°E. This can account for the lower K_2O and less-enriched heavy isotopes compared to Mayes Smt without having to appeal to a significantly different bulk mantle composition.

Narrowgate isotopically closely resembles Bouvet Is and EMII basalts (Figs. 8a and b), with Na_8 (2.96) close to the SWIR average (3.10). The enormous Mayes Smt axial volcano, compared to the deep rift valley at Narrowgate, as well as the large differences in Fe_8 all suggest shallower mantle upwelling at Mayes Smt to produce the volume of melt required, while the higher K_2O and water contents at Narrowgate suggest that melting is capped deeper there, and thus the enriched low temperature melting component dominates the isotopic composition, which lies at the EMII endmember of the global isotopic array – which also dominates the Bouvet lavas. The very low Fe_8 (5.56 wt.%), however, would seem

Please cite this article in press as: Yu, X., Dick, H.J.B. Plate-driven micro-hotspots and the evolution of the Dragon Flag melting anomaly, Southwest Indian Ridge. Earth Planet. Sci. Lett. (2019), https://doi.org/10.1016/j.epsl.2019.116002

inconsistent with this. However, the simple Na_8-Fe_8 logic varying systematically with potential temperature and mantle composition (Klein and Langmuir, 1987; Dick and Zhou, 2015) should not be extended to where you are dealing with an alkaline basalt with an average of 1.26 wt.% K_2O and 0.74 wt.% H_2O generated in a two (or more) component mantle, and an Bouvet Hotspot end-member isotopic composition. Water, potassium and soda all strongly affect the partitioning of iron and magnesium between melt and olivine (e.g., Liu et al., 2018), which suggests that the magma has been generated largely by melting an early melting pyroxenite component. Thus, the simple Klein and Langmuir (1987) and Dick and Zhou (2015) interpretation should not be stretched so far as to account for the differences with tholeiitic MORB.

The large volume of the basalts generated at the segment-scale micro hotspots, then is attributed to the wide spacing of these segments (see also Sauter et al., 2001), which results in an exceptionally wide zones of mantle melt contribution. We note here that isotopically, all three of our western micro hotspots lie on a mixing line between Bouvet and DMM. In summary, while there may be some increase in the proportion of the enriched component in the mantle source, which dominates the Bouvet magmas, much of the difference in the isotopic composition and major element chemistry of Mayes Smt, Narrowgate and 16°E Segments can be accounted for by tectonic process rather than by large changes in the bulk composition of the underlying mantle.

The very high Na_8 and extremely depleted isotopic composition of the 63.9° basalts is highly significant, as it suggests that there is not a significant enriched component in the underlying mantle, but rather that the mantle source is more fertile (diopside rich) than typical DMM compositions. The great mean depth (~4.7 km) and thin ocean crust suggest an unusually cold mantle, and hence the magmas should reflect this (Meyzen et al., 2003), but clearly any low-melting enriched component must have been previously removed if it was once there. This region of the SWIR is where it propagated into lithosphere generated at the Central and Southeast Indian Ridge, and thus renewed melting of the underlying asthenosphere, that first occurred beneath those ridges, providing a simple explanation for the discontinuity in basalt compositions across the triple junction there. The elevated sodium may support this low-degree renewed melting beneath the SWIR near the triple junction.

7. Multi-segment scale micro hotspots

7.1. Atlantis Bank Supersegment

We recognize a new multi-segment melting anomaly, the Atlantis Bank Supersegment. It lies between the Atlantis II and Melville FZ's extending 400 km from 57.1° to 60.7°E (Fig. 9). Average RMBA between the Atlantis II and Melville FZ is close to 20 mGal's lower than between the Melville FZ (60.7°E) and 65.5°E (Rommevaux-Jestin et al., 1997), consistent with thicker crust along the Supersegment. Similar to Dragon Flag, there was a sharp increase in magmatic activity, beginning at its center adjacent to the Novara FZ at ~14.1 Ma (magnetic Anomaly 5ADn). This activity rapidly advanced to the west and east (black dotted line in Fig. 9a), though slowly to the east at first and then rapidly at an overall rate of ~12.5 mm/yr. This created a broad swath of ~1-km excess elevated bathymetry that varies from ~265 km wide at 58.9°E to 130 km at 60.1°E (~120 km). Like the Dragon Flag Anomaly, this cuts across and terminates the traces of the non-transform discontinuities between the Atlantis II, Novara, and Melville FZ's. These discontinuities (N1A and M1N in Fig. 9a) are ~1.5 km deep N-S troughs that can be traced out to the Rodriguez Triple Junction traces far to the north and south. Several such troughs to the west, including A1G, pass uninterrupted through the rift mountains and across the ridge axis indicating that there was no corresponding sudden increase in magma flux. Like Dragon Flag, the anomalous terrain represents simultaneous eruption along multiple magmatic segments, linked by small non-transform discontinuities (Fig. 9c). Its dimensions are complicated by the effect of a ~19.5 Ma +10° spreading direction change (Baines et al., 2007). The latter put the transforms into transtension, with the intervening volcanic segments propagating under the enhanced melt flux west to create V-shaped rift-mountain trends, increasing their total length ~40-50 km.

The eastern transverse ridge flanking the Atlantis II FZ has the most abundant exposures of gabbroic crust anywhere on the global ridge system, including the Atlantis Bank Oceanic Core Complex, from which the name of the Supersegment is derived. This clearly demonstrates far more robust magmatism than occurred along most of the SWIR. Excluding the Atlantis II FZ, only 4% of the rock dredged along the SWIR is gabbro, while 17% from the Atlantis II Transform wall is gabbro. Atlantis Bank, lying just within the melting anomaly, exposes a >1,508-m thick 660-km^2 gabbro massif flanking the transform (Dick et al., 2019). Drilling there has not yet reached primitive gabbros complimentary to the original overlying basalts, so the total lower crustal section is likely much thicker (Dick et al., JGR, accepted). Thus, both bathymetric and geologic data show the 57°-60°E Melting Anomaly crust is unusually thick.

Unlike the Dragon Flag Anomaly, the ridge axis is deep (~4500 to 5000-m), consistent with very alumina-rich fertile mantle (Zhou and Dick, 2013), but has ~1-km excess relief in relation to the older seafloor to the north and south. The largest local volcanic high shoals to 3,000 m near the eastern intersection with the Novara FZ. Despite a strong ridge obliquity, the Novara-Melville segment consists of 4 en-echelon 2nd-order ridge segments, rather than an amagmatic spreading center; as found for similar oblique segments along the SWIR. This is consistent with a high present-day magma budget, centered not at the eastern end of the segment, as at Dragon Flag, but at 58.7°E where the melting anomaly initiated.

Like the Dragon Flag Supersegment, the Atlantis Bank Supersegment consists of MORB rather than alkali basalt. Unlike Dragon Flag, the basalt has high Na_8 and low Fe_8 (Fig. 7), while the spatially associated mantle peridotites are aluminous lherzolites with 6.2% clinopyroxene (3.0 1sd, N = 15), while the peridotites from the western wall of the fracture zone have only 3.6% Cpx (1.9 1sd, N = 27) (Johnson and Dick, 1992). The Atlantis Bank Supersegment is isotopically unique, with very unradiogenic Pb, but rather typical depleted MORB $^{87}Sr/^{86}Sr$ (0.70279 ±0.00009, n = 16), representing some of the most depleted basalts on the global ridge system, sharply contrasting to MORB dredge to the east and the west.

7.2. Multi-segment micro hotspots — discussion

Multi-segment melting anomalies cannot be explained by focused delivery of low degree melts through thick lithosphere from a broad zone of melt contribution. Excess volcanism occurred simultaneously along several 100's of kilometers along these Supersegments, eliminating major axial discontinuities, and crossing transforms. Moreover, the lavas are low-potassium tholeiites representing high-degree melting of a multi-component mantle, not low degree capped by a thick lithosphere as at Narrowgate. The propagation of these anomalies, however, like the segment scale micro-hotspots, was controlled by lithospheric stresses, and neither are related to an adjacent mantle hotspot.

The Atlantis Bank melting anomaly is represented by low-potassium isotopically extremely depleted basalts confined entirely within the bounds of the Atlantis II and Melville FZ's (Fig. 7c and d). The high Na_8 and moderate Fe_8, which lies, close to the cen-

Please cite this article in press as: Yu, X., Dick, H.J.B. Plate-driven micro-hotspots and the evolution of the Dragon Flag melting anomaly, Southwest Indian Ridge. Earth Planet. Sci. Lett. (2019), https://doi.org/10.1016/j.epsl.2019.116002

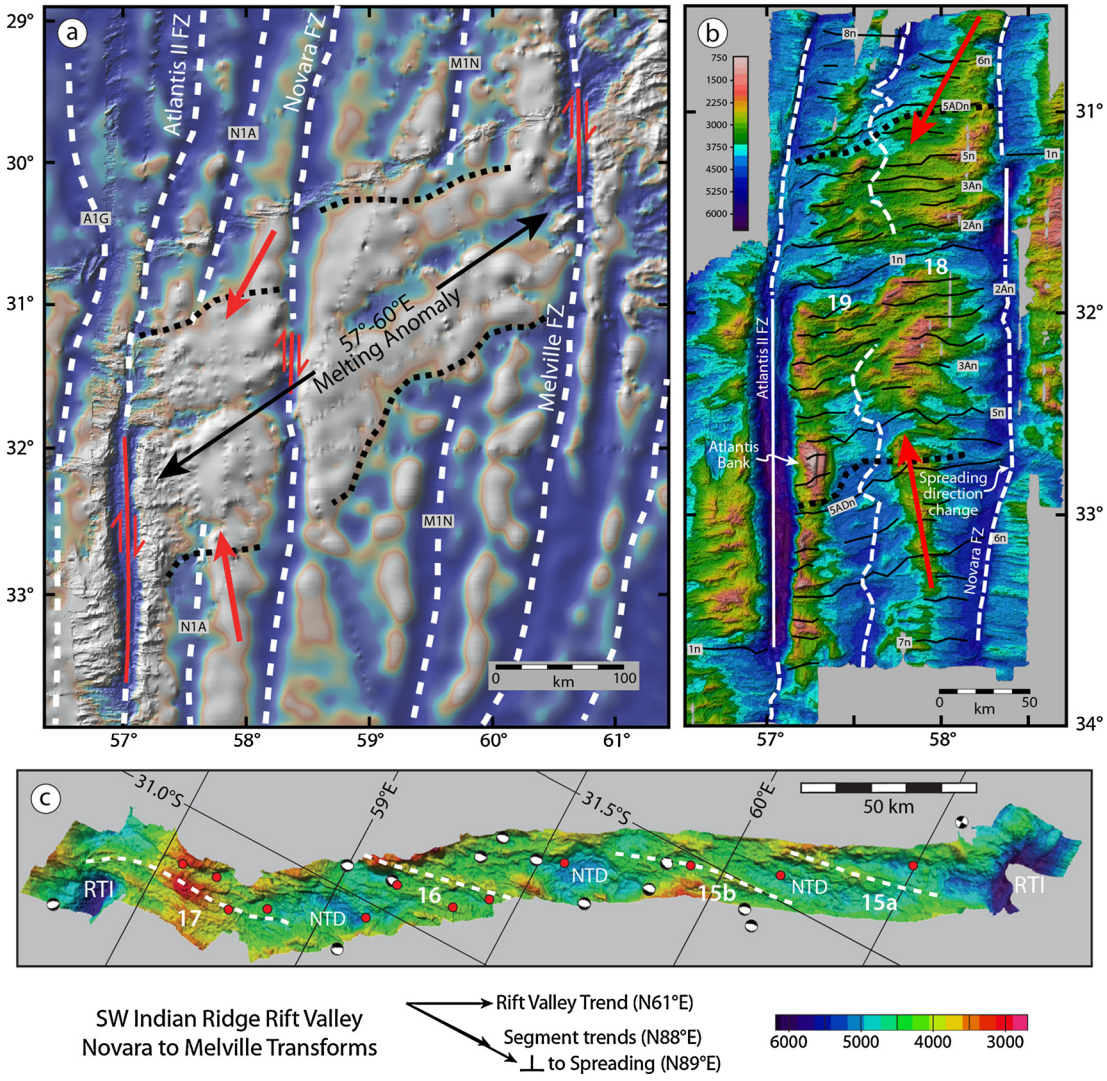

Fig. 9. Atlantis Bank Melting Anomaly. (a) Shaded bathymetric map of the anomaly from GeoMapApp. Heavy black dotted line outlines the extent of the anomaly, while heavy red arrows indicate westward V-shaped trends due to 2nd-order volcanic segment migration following the 19.5 Ma 10° spreading direction rotation. Heavy dashed white lines show the traces of long-lived discontinuities and fracture zones, and red lines show active transform faults. (b) RV Yokosuka Cruise MODE 98, RV Kaire Cruise KR00-06 (2000), RV Yokosuka Cruise YK01-14 Multi-beam bathymetry (Arai et al., 2001; Kinoshita et al., 2001; Matsumoto et al., 2001). (c) Shaded bathymetric map of the SWIR from the Novara to the Melville FZ (Arai et al., 2001). CMT solutions for earthquakes downloaded from GeoMapApp, and dredge locations are from PetDB. Segment numbering modified from Cannat et al. (1999).

ter of the global array, would then be best explained by a highly fertile but isotopically depleted mantle composition that was entrained in the melting column some at ~14 Ma. A large mass of basaltic crust, with high Na_8 associated with a fertile aluminous mantle residue cannot be simply explained by a thermal anomaly, but is consistent with excess melting due to the initiation of melting deeper in the melting column due to its fertile composition.

The Dragon Flag and Atlantis Bank anomalies are very similar in their size judged from their bathymetric expression and associated gravity anomies — yet they have very different isotopic compositions, and the major element signals (Na_8-Fe_8) are radically different (Table 1), despite both representing low-potassium tholeiites. Following Klein and Langmuir (1987) the Atlantis Bank Supersegment should have a crustal thickness ~3 km, while Segment 17 should be <2-km, while Dragon Flag would have a 4-km thick crust. Given the very high soda content of these basalts, it is clear that the mantle compositions are far more fertile than that used by Klein and Langmuir in their modeling, and that they are also very different from each other, as would be predicted from the isotopic composition of their respective lavas. Thus, as suggested by Anderson (2006) we find that our multi-segment micro hotspots reflect the intrinsic chemical and lithologic heterogeneity of the upper mantle, due to subduction and continental breakup, where the magnitude of magmatism reflects the fertility, not the absolute temperature of the asthenosphere.

Declaration of competing interest

The authors declare that they have no known competing financial interests or personal relationships that could have appeared to influence the work reported in this paper.

Acknowledgements

The authors would like to express great thanks to Chengguang Sun, Emmanuel Codillo and Changgui Gao from Woods Hole Oceanographic Institute for helpful discussion, to Wang Wei, Wu Xichang and Wang Jianqiang for their kind help in chemical analysis. This work was supported by fundings from the National Natural Science Foundation of China [41872242, 91951201, 41830540, 91858214], the Natural Science Foundation Project of Zhejiang

[LY17D02001], the Projects of China Ocean Mineral R&D Association (DY135-S2-1-02) and partial support from the US National Science Foundation (NSF OCE MG&G #1434452).

Appendix. Supplementary material

Supplementary material related to this article can be found online at https://doi.org/10.1016/j.epsl.2019.116002.

References

Anderson, D.L., 2006. Speculations on the nature and cause of mantle heterogeneity. Tectonophysics 416, 7–22.

Arai, S., Dick, H.J.B., MODE 2000 Scientific Party, 2001. Cruise Report MODE 2000 (Kairei/Kaiko KR00-06) Investigation of Atlantis Bank and the SW Indian Ridge from 57°E to 62°E. Japan Marine Science and Technology Center, Yokosuka, Japan. 337 p.

Baines, A.G., Cheadle, M.J., Dick, H.J.B., Hosford Sheirer, A., John, B.E., Kusznir, N., Matsumoto, T., 2007. Evolution of the Southwest Indian Ridge from 55 degrees 45′E to 62 degrees E; changes in plate-boundary geometry since 26 Ma. Geochem. Geophys. Geosyst. 8. https://doi.org/10.1029/2006GC001559.

Ben Othman, D., Polve, M., Allegre, C.J., 1984. Nd-Sr isotopic composition of granulites and constraint on the evolution of the lower continental crust. Nature 307, 510–515.

Breton, T., Nauret, F., Pichat, S., Moine, B., Moreira, M., Rose-Koga, E.F., Auclair, D., Bosq, C., Wavrant, L.-M., 2013. Geochemical heterogeneities within the Crozet hotspot. Earth Planet. Sci. Lett. 376, 126–136. https://doi.org/10.1016/j.epsl.2013.06.020.

Cannat, M., Rommevaux-Jestin, C., Sauter, D., Deplus, C., Mendel, V., 1999. Formation of the axial relief at the very slow spreading Southwest Indian Ridge (49° to 69°E). J. Geophys. Res. 104, 22,825–22,843. https://doi.org/10.1029/1999JB900195.

Collins, A.S., Windley, B.F., 2002. The tectonic evolution of central and northern Madagascar and its place in the final assembly of Gondwana. J. Geol. 110, 325–339.

Dalton, C.A., Langmuir, C.H., Gale, A., 2014. Geophysical and geochemical evidence for deep temperature variations beneath mid-ocean ridges. Science 344, 80.

Danyushevsky, L.V., Plechov, P., 2011. Petrolog3: integrated software for modeling crystallization processes. Geochem. Geophys. Geosyst. 12, Q07021. https://doi.org/10.1029/2011GC003516.

Dick, H.J.B., Lin, J., Schouten, H., 2003. An ultraslow-spreading class of ocean ridge. Nature 426, 405–412.

Dick, H.J.B., MacLeod, C.J., Blum, P., et al., 2019. Dynamic accretion beneath a slow-spreading ridge segment: IODP Hole 1473A and the Atlantis Bank Oceanic Core Complex. J. Geophys. Res., Solid Earth. https://doi.org/10.1029/2018JB016858.

Dick, H.J.B., Zhou, H.Y., 2015. Ocean rises are products of variable mantle composition, temperature and focused melting. Nat. Geosci. 8, 68–74.

Doucet, S., Weis, D., Scoates, J., Debaille, V., Giret, A., 2004. Geochemical and Hf–Pb–Sr–Nd isotopic constraints on the origin of the Amsterdam–St. Paul (Indian Ocean) hotspot basalts. Earth Planet. Sci. Lett. 218, 179–195.

Duncan, R.A., 1981. Hot spots in the southern oceans—an absolute frame of reference for the motion of the Gondwana continents. Tectonophysics 74, 29–42.

Dupré, B., Allègre, C.J., 1983. Pb-Sr isotope variation in Indian Ocean basalts and mixing phenomena. Nature 303, 142–146.

Font, L., Murton, B.J., Roberts, S., et al., 2007. Variations in melt productivity and melting conditions along SWIR (70°E–49°E): evidence from olivine-hosted and plagioclase-hosted melt inclusions. J. Petrol. 48, 1471–1494.

Gao, C., Dick, H.J.B., Liu, Y., Zhou, H., 2016. Melt extraction and mantle source at a Southwest Indian Ridge Dragon Bone amagmatic segment on the Marion Rise. Lithos, 49–60.

Gautheron, C., Moreira, M., Gerin, C., Tassan-Got, L., Bezos, A., Humler, E., 2015. Constraints on the DUPAL anomaly from helium isotope systematics in the Southwest Indian mid-ocean ridge basalts. Chem. Geol. 417, 163–172.

Georgen, J.E., Lin, J., Dick, H.J.B., 2001. Evidence from gravity anomalies for interactions of the Marion and Bouvet hotspots with the Southwest Indian Ridge: effects of transform offsets. Earth Planet. Sci. Lett. 187, 283–300.

Hart, S.R., 1984. A large-scale isotope anomaly in the Southern Hemisphere mantle. Nature 309, 753–757.

Hawkesworth, C.J., Erlank, A.J., Kempton, P.D., Waters, F.G., 1990. Mantle metasomatism: isotope and trace element trends in xenoliths from Kimberley, South Africa. Chem. Geol. 85, 19–34.

Janney, P.E., le Roex, A.P., Carlson, R.W., 2005. Hafnium isotope and trace element constraints on the nature of mantle heterogeneity beneath the central Southwest Indian Ridge (13°E to 47°E). J. Petrol. 46, 2427–2464.

Johnson, K.T.M., Dick, H.J.B., 1992. Open system melting and the temporal and spatial variation of peridotite and basalt compositions at the Atlantis II fracture zone. J. Geophys. Res. 97, 9219–9241.

Kempton, P.D., Pearce, J.A., Barry, T.L., Fitton, J.G., Langmuir, C., Christie, D.M., 2002. Sr-Nd-Pb-Hf isotope results from ODP Leg 187: evidence for mantle dynamics of the Australian-Antarctic Discordance and origin of the Indian MORB source. Geochem. Geophys. Geosyst. 3 (12), 1074. https://doi.org/10.1029/2002GC000320.

Kinoshita, H., Dick, H.J.B., Yokosuka/Shinkai 6500 Scientific Party, 2001. MODE'98 Leg 4 Cruise Report - Atlantis II Fracture Zone, Nov. - Dec. 1998. Japan Marine Science and Technology Center, Yokosuka, Japan. 236 p.

Klein, E.M., Langmuir, C.H., 1987. Global correlations of ocean ridge basalt chemistry with axial depth and crustal thickness. J. Geophys. Res. 92, 8089–8115.

le Roex, A.P., Chevallier, L., Verwoerd, W.J., Barends, R., 2012. Petrology and geochemistry of Marion and Prince Edward Islands, Southern Ocean: magma chamber processes and source region characteristics. J. Volcanol. Geotherm. Res. 223–224, 11–28.

le Roex, A.P., Dick, H.J.B., Fisher, R.L., 1989. Petrology and geochemistry of MORB from 25°E to 46°E along the Southwest Indian Ridge: evidence for contrasting styles of mantle enrichment. J. Petrol. 30, 947–986.

le Roex, A.P., Dick, H.J.B., Watkins, R.T., 1992. Petrogenesis of anomalous K-enriched MORB from the Southwest Indian Ridge: 11°53′E to 14°38′E. Contrib. Mineral. Petrol. 110, 253–268.

Liu, L.P., Hu, X.M., Liu, X., 2018. MgO partition between olivine and K2O-rich silicate melt: geothermometers applicable to high potassium magmas. J. Asian Earth Sci. 166, 181–194.

Mahoney, J.J., Natland, J.H., White, W.M., Poreda, R., Bloomer, S.H., Fisher, R.L., Baxter, A.N., 1989. Isotopic and geochemical provinces of the western Indian Ocean spreading centers. J. Geophys. Res., Solid Earth 94, 4033–4052.

Mahoney, J., Nicollet, C., Dupuy, C., 1991. Madagascar basalts: tracking oceanic and continental sources. Earth Planet. Sci. Lett. 104, 350–363.

Mahoney, J., le Roex, A.P., Peng, Z., Fisher, R.L., Natland, J.H., 1992. Southwestern limits of Indian Ocean Ridge Mantle and the origin of low $^{206}Pb/^{204}Pb$ mid-ocean ridge basalt: isotope systematics of the central Southwest Indian Ridge (17°-50°E). J. Geophys. Res., Solid Earth 97, 19771–19790.

Matsumoto, T., Dick, H.J.B., Miyashita, S., John, B.E., Maeda, J., Kvassnes, A., Morishita, T., Cheadle, M.J., Ohtomo, Y., Kumagai, H., Miranda, E.A., Warren, J.M., Baines, A.G., 2001. RV Yokosuka MODE 2001 Cruise Report. JAMSTEC.

Mendel, V., Sauter, D., Rommevaux-Jestin, C., Patriat, P., Lefebvre, F., Parson, L.M., 2003. Magmato-tectonic cyclicity at the ultra-slow spreading Southwest Indian Ridge: evidence from variations of axial volcanic ridge morphology and abyssal hills pattern. Geochem. Geophys. Geosyst. 4, 9102. https://doi.org/10.1029/2002GC000417.

Meyzen, C.M., Ludden, J.N., Humler, E., Luais, B., Toplis, M.J., Mevel, C., Storey, M., 2005. New insights into the origin and distribution of the DUPAL isotope anomaly in the Indian Ocean mantle from MORB of the Southwest Indian Ridge. Geochem. Geophys. Geosyst. 6, Q11K11. https://doi.org/10.1029/2005GC000979.

Meyzen, C.M., Toplis, M.J., Humler, E., Ludden, J.N., Mével, C., 2003. A discontinuity in mantle composition beneath the Southwest Indian Ridge. Nature 421, 731–733.

Miller, C., Schuster, R., Klotzli, U., Frank, W., Purtscheller, F., 1999. Post-collisional potassic and ultrapotassic magmatism in SW Tibet; geochemical and Sr-Nd-Pb-O isotopic constraints for mantle source characteristics and petrogenesis. J. Petrol. 40, 1399–1424.

Niu, X., Ruan, A., Li, J., Minshull, T.A., Sauter, D., Wu, Z., Qiu, X., Zhao, M., Chen, Y.J., Singh, S., 2015. Along-axis variation in crustal thickness at the ultraslow spreading Southwest Indian Ridge (50°E) from a wide-angle seismic experiment. Geochem. Geophys. Geosyst. 16. https://doi.org/10.1002/2014GC005645.

Rehkämper, M., Hofmann, A.W., 1997. Recycled ocean crust and sediment in Indian Ocean MORB. Earth Planet. Sci. Lett. 147, 93–106.

Rommevaux-Jestin, C., Deplus, C., Patriat, P., 1997. Mantle Bouguer anomaly along an ultraslow-spreading ridge: implications for accretionary processes and comparison with results from central Mid-Atlantic Ridge. Mar. Geophys. Res. 19, 481–503.

Sauter, D., Cannat, M., Meyzen, C., 2009. Propagation of a melting anomaly along the ultraslow Southwest Indian Ridge between 46°E and 52°20′E: interaction with the Crozet hotspot? Geophys. J. Int. 179, 687–699.

Sauter, D., Cannat, M., Roumejon, S., et al., 2013. Continuous exhumation of mantle-derived rocks at the Southwest Indian Ridge for 11 million years. Nat. Geosci. 6, 314–320.

Sauter, D., Patriat, P., Rommevaux-Jestin, C., Cannat, M., Briais, A., Gallieni Shipboard Scientific Party, 2001. The Southwest Indian Ridge between 49°15′E and 57°E: focused accretion and magma redistribution. Earth Planet. Sci. Lett. 192, 303–317.

Schlindwein, V., Schmid, F., 2016. Mid-ocean-ridge seismicity reveals extreme types of ocean lithosphere. Nature 535, 276–279.

Snow, J.E., 1993. The isotope geochemistry of abyssal peridotites and related rocks. MIT/Woods Hole Joint Program in Marine Geology and Geophysics. Woods Hole Oceanographic Institution/Massachusetts Institute of Technology, Woods Hole, MA.

Standish, J.J., 2006. The Influence of Ridge Geometry at the Ultraslow-Spreading Southwest Indian Ridge (9°-25°E): Basalt Composition Sensitivity to Variations in Source and Process. The WHOI Department of Geology and Geophysics and

the MIT Department of Earth and Planetary Sciences, Woods Hole Oceanographic Institution and the Massachusetts Institute of Technology, p. 286.

Standish, J.J., Dick, H.J.B., Michael, P.J., Melson, W.G., O'Hearn, T., 2008. MORB generation beneath the ultraslow spreading Southwest Indian Ridge (9-25°E): major element chemistry and the importance of process versus source. Geochem. Geophys. Geosyst. 9, Q05004. https://doi.org/10.1029/2008GC001959.

Standish, J.J., Sims, K.W.W., 2010. Young off-axis volcanism along the ultraslow-spreading Southwest Indian Ridge. Nat. Geosci. 3, 286–292.

Stern, R.J., 1994. Arc assembly and continental collision in the Neoproterozoic East African Orogen: implications for the consolidation of Gondwanaland. Annu. Rev. Earth Planet. Sci. 22, 319–351.

Sun, S., McDonough, W.F., 1989. Chemical and isotopic systematics of oceanic basalt. In: Saunders, A.D., Norry, M.J. (Eds.), Magmatism in the Ocean Basins. Geol. Soc. Spec. Pub. 42, 313–345.

Yang, A.Y., Zhao, T.-P., Zhou, M.-F., Deng, X.-G., 2017. Isotopically enriched N-MORB - a new geochemical signature of off-axis plume-ridge interaction: a case study at 50°28′E, Southwest Indian Ridge. J. Geophys. Res., Solid Earth 121. https://doi.org/10.1002/2016JB013284.

Zhang, T., Jian, L., JinYao, G., 2011. Interactions between hotspots and the Southwest Indian Ridge during the last 90 Ma: implications on the formation of oceanic plateaus and intra–plate seamounts. Sci. China Earth Sci. 54, 1177–1188.

Zhou, H., Dick, H.J.B., 2013. Thin crust as evidence for depleted mantle supporting the Marion Rise. Nature 494, 195–200. https://doi.org/10.1038/nature11842.

Zindler, A., Hart, S., 1986. Chemical geodynamics. Annu. Rev. Earth Planet. Sci. 14, 493–571.

Please cite this article in press as: Yu, X., Dick, H.J.B. Plate-driven micro-hotspots and the evolution of the Dragon Flag melting anomaly, Southwest Indian Ridge. Earth Planet. Sci. Lett. (2019), https://doi.org/10.1016/j.epsl.2019.116002